processes

MDPI

Article

Analyzing Support Stability of Deep Shaft Based on Plastic Softening and Dilatancy of Hard Rock Mass

Xingdong Zhao, Shaolong Qin *, Yangyang Li, Wenlong Yu and Tong Wu

School of Resources and Civil Engineering, Northeastern University, Shenyang 110819, China
* Correspondence: 2110406@stu.neu.edu.cn

Abstract: To explore the stability analyses and control methods for surrounding rocks in deep hard rock shafts, this paper is based on field engineering geological surveys and laboratory rock mechanics tests and relies on the main shaft being constructed in the Shaling Gold Mine of China as the engineering background. The quality of the rock mass is evaluated by the Q system, rock mass rating (RMR) and geological strength index (GSI). The mechanical parameters of the surrounding rock mass of the shaft are calculated by using the generalized Hoek–Brown failure criterion, and the main support system is determined based on the rock mass classification system. Based on the finite element method, a two-dimensional plane strain model is constructed to analyze and evaluate the deformation and plastic region range of surrounding rocks for different support systems. On this basis, considering the dilatancy and plastic softening characteristics of hard rock masses, an analytical solution of the stress, strain and plastic region radius of hard rock around shafts in homogeneous media is proposed. Finally, the plastic region of the surrounding rock is measured by the P-wave velocity test method. The results show that after considering the dilatancy and plastic softening characteristics of the rock mass, the numerical simulation, theoretical analytical solution and measured results are basically consistent, and the proposed support system can effectively ensure the stability of the shaft.

Keywords: dilatancy; plastic softening; support system; numerical simulation; analytical solution; P-wave velocity test; plastic region

check for updates

Citation: Zhao, X.; Qin, S.; Li, Y.; Yu, W.; Wu, T. Analyzing Support Stability of Deep Shaft Based on Plastic Softening and Dilatancy of Hard Rock Mass. *Processes* **2023**, *11*, 186. https://doi.org/10.3390/pr11010186

Academic Editor: Chin-Hyung Lee

Received: 19 November 2022
Revised: 1 January 2023
Accepted: 3 January 2023
Published: 6 January 2023

Copyright: © 2023 by the authors. Licensee MDPI, Basel, Switzerland. This article is an open access article distributed under the terms and conditions of the Creative Commons Attribution (CC BY) license (https://creativecommons.org/licenses/by/4.0/).

1. Introduction

With the depletion of shallow mineral resources, China has gradually entered the deep mining stage. An increase in mining depth leads to an increase in situ stress, while high situ stress leads to wall caving and rock burst, which restrict the construction and production of deep shafts [1]. Thus, it is necessary to analyze the stability of a sinking shaft to ensure the safe and efficient production of the mine [2–5].

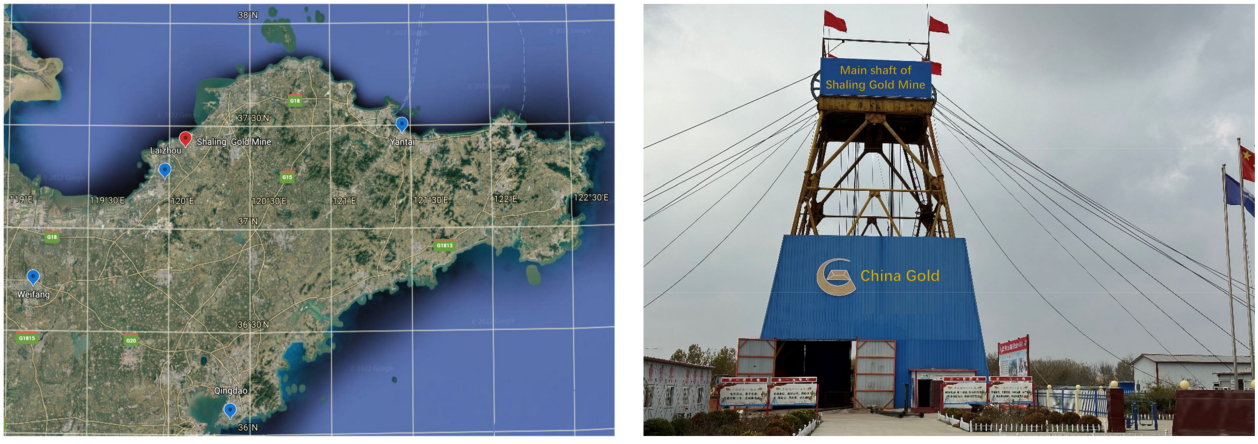
At present, the stability analysis methods in rock mass engineering that can be used for reference in shafts generally include the following: engineering analogy, analytical, numerical simulation, micro seismic and deformation monitoring, etc. For complex rock engineering problems, the successful experience of related or similar engineering cases is an important reference. With the introduction of advanced mathematical theories into the surrounding rock quality grading and evaluation system, new surrounding rock quality grading methods have emerged, such as the establishment of a rock mass quality evaluation method based on the BP neural network principle [6,7]. A comprehensive evaluation model for rock mass quality was developed based on fuzzy mathematics theory [8,9]. In the analysis of the stability of the surrounding rock, the analytical method is mostly used to solve the stress and deformation of a circular tunnel. Although the analytical method has the advantages of high accuracy, fast analysis speed and the ease of conducting regularity studies, it produces certain errors in the solution of underground engineering,

such as complex stress conditions and large burial depths [10–13]. The numerical simulation calculation can comprehensively consider a variety of factors, and the calculation results are intuitive. It has been increasingly widely used in the study of underground rock mass engineering stability and has become an important research method in rock mechanics [14–18]. At present, the commonly used numerical analysis methods mainly include finite element, finite difference, block element, boundary element, DDA, discrete element, etc. The finite difference method is often used for the stability analysis of surrounding rocks with complex geological structures and various materials in sections [19]. The block element method is mainly applicable to the stability analysis of rock masses with geological structural planes [20]. The boundary element method can be used to calculate the large deformation of the surrounding rock of caverns in jointed rock masses [21]. Wu, A. used the DDA method to analyze the problems of tunnel excavation and the open excavation of slopes [22]. Tan, Y.L. studied the influence of full-length bolts on the stability of jointed surrounding rock by using the discrete element method [23].

As mentioned above, there are abundant methods for the stability analysis of shafts, but each method still has some limitations, especially for the stability analysis of surrounding rocks in deep shafts. Due to the influence of special geological conditions such as high in situ stress, high confined water, high rock temperature and high disturbance stress, the stability analysis of surrounding rocks via a single method cannot reflect the true state of the surrounding rocks. In the existing stability analysis of hard rock surrounding rocks, the plastic softening and volume-expansion properties of hard rock masses under high stress conditions have not been comprehensively considered. Thus, in this paper, the plastic softening and dilatancy properties of hard rock masses under high in situ stress are analyzed synthetically based on field measurements, theoretical analyses and numerical simulations to reveal the real stability of deep shafts.

2. Field and Laboratory Studies

The main shaft of the Shaling Gold Mine is located in Laizhou City, Shandong Province, China. The geomorphic unit belongs to the intersection of hills and alluvial plains, as shown in Figure 1. The designed production capacity of the mine is 12,000 t/d. The main shaft is a circular section with a diameter of 7.8 m, with a ground elevation of +19.0 m, shaft bottom elevation of −1539 m and shaft depth of 1558 m [24]. The area is characterized by a simple formation, well-developed fault structures and the wide distribution of magmatic rocks. The lithology of the hanging wall in the mine is mainly gabbro, while the footwall is pyrite sericite fractured rock, pyrite sericite–granitic fractured rock and pyrite sericite-treated granite, and the remaining rocks are adamellite, as shown in Figure 2.



(**a**) (**b**)

Figure 1. (**a**) Location map of the main shaft of the Shaling Gold Mine; (**b**) construction site of the main shaft.

According to the joint survey results of the main shaft at a depth of −1465 m on the site, the joint opening of the surrounding rock is 0.1~0.25 mm, mainly filled with quartz, the main joint group is slightly rough, and the water yield of the joint surface is large. Figure 3 shows the stereographic projection and rose diagram of the main shaft surrounding rock at −1465 m. Figure 3 shows that the dominant joint group of the surrounding rock is one group, with a dip of 310~320°, a dip of 70~80° and an average spacing of 0.43 m. The RQD calculated via the scan line method is 87%.

In light of the distribution law of in situ stress measured via hydraulic fracturing, the deep in situ stress field in the main shaft area is dominated by horizontal stress, and the vertical principal stress is the intermediate stress. The direction of the maximum horizontal principal stress is NW65°. The maximum horizontal principal stress of the surrounding rock of the shaft at a depth of −1465 m is 45.8 MPa, the minimum horizontal principal stress is 37.6 MPa, and the vertical principal stress is 40.5 MPa, as shown in Figure 4.

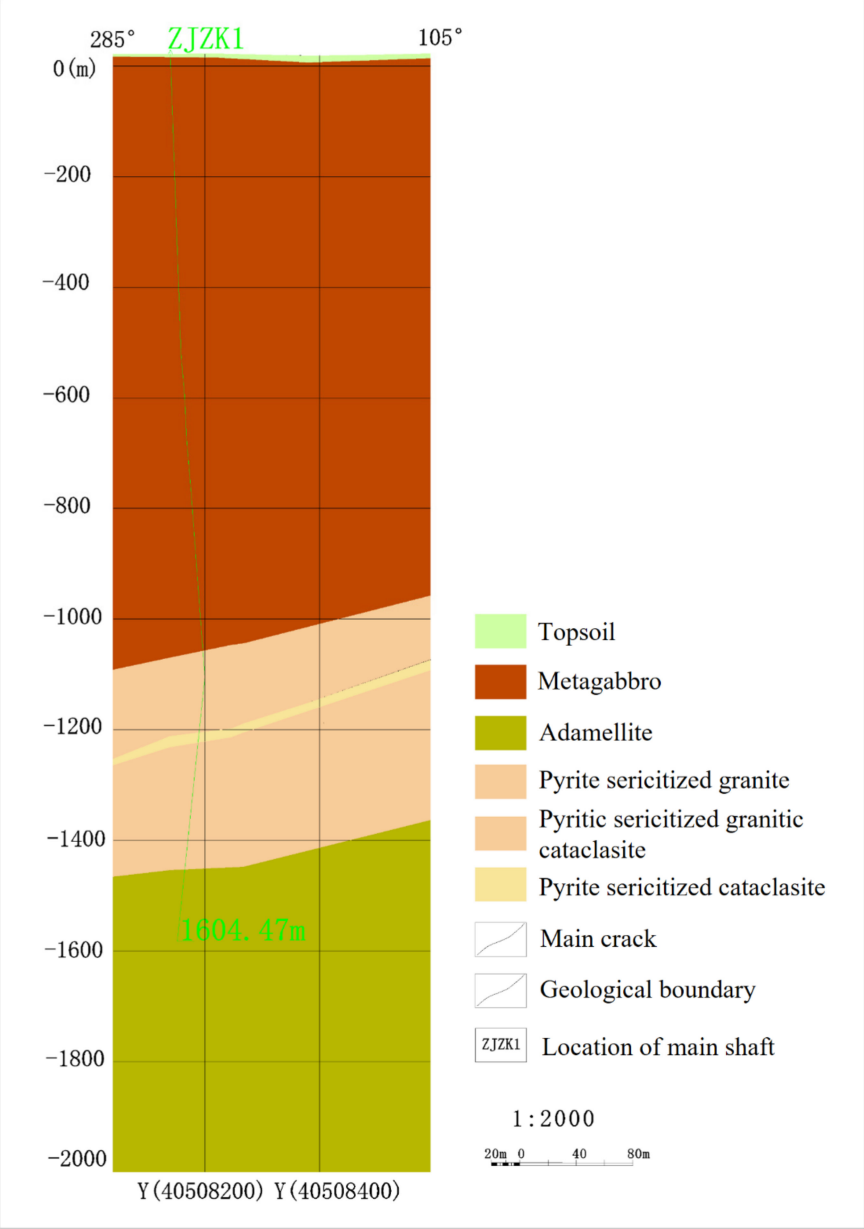
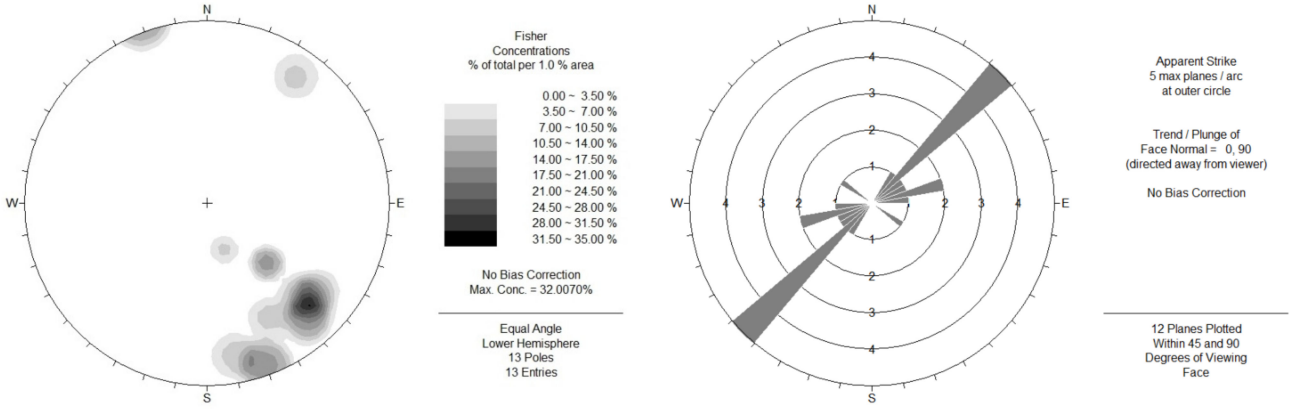


Figure 2. Borehole histogram of ZJZK-1.



(**a**) (**b**)

Figure 3. (**a**) Contour plot; (**b**) rosette plot.

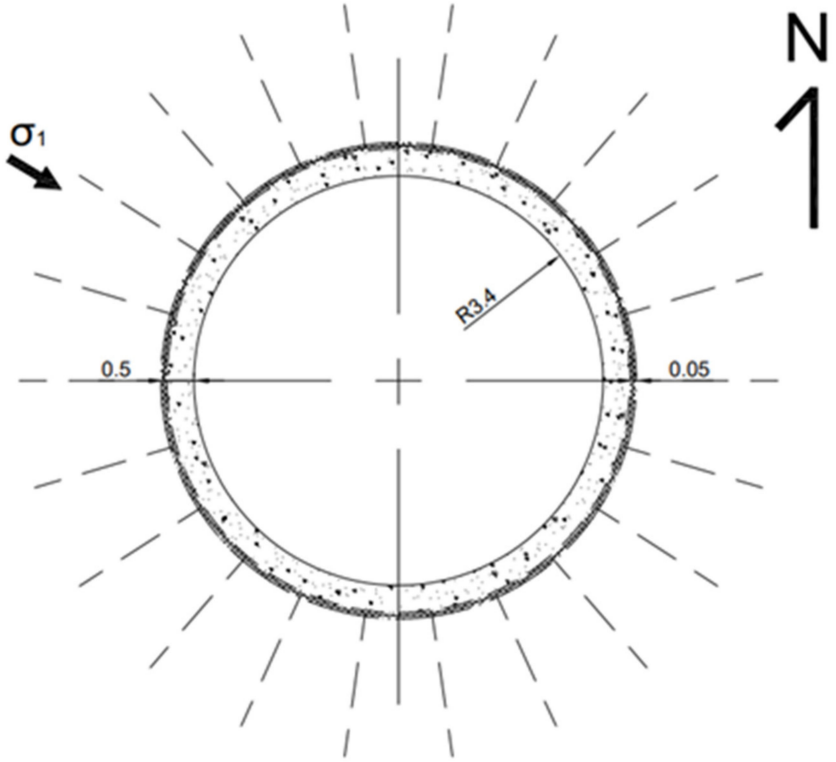


Figure 4. Direction of maximum horizontal principal stress of the shaft.

Rock samples with good integrity were collected from the main shaft at −1465 m. According to the laboratory testing on intact rock samples following the ISRM (1981) recommended methods, the physical and mechanical properties of the rock are given in Table 1.

Table 1. Intact rock mean parameters.

Rock	Density g/cm^3	σ_t/MPa	UCS/MPa	E/GPa	μ	c/MPa	φ/°
Granite	2.66	9.76	149.7	68.64	0.20	21.74	49.2

The Q system was proposed by the Norwegian Geotechnical Institute (NGI) based on the case history of approximately 200 tunnels and chambers [25]. Rock mass qual-

ity is described using six parameters: RQD, joint set number (J_n), joint roughness (J_r), joint alteration (J_a), joint water reduction coefficient (J_w) and stress reduction coefficient (SRF). By combining these six parameters, the Q rating is derived from the following expression [26,27]:

$$Q = \frac{RQD}{J_n} \times \frac{J_r}{J_a} \times \frac{J_w}{SRF} \quad (1)$$

Based on the field investigation results, the evaluation results of the Q classification of the surrounding rock at a depth of −1465 m in the Shaling main shaft calculated according to the above expression are shown in Table 2.

Table 2. Evaluation results of the Barton rock mass classification (Q).

Depth/m	RQD	J_n	J_r	J_a	J_w	SRF	Q	Rating	Rock Quality
−1465	87	3	3	5.0	1.0	10	1.74	III	poor

The RMR system was originally developed by Bieniawski based on shallow tunnels in sedimentary rocks. It uses six parameters: the uniaxial compressive strength (UCS) of the intact rock material, the rock quality index (RQD), joint spacing, joint condition, groundwater condition and correction factor [28]. The rock mass quality evaluation results using the RMR system are shown in Table 3.

Table 3. Classification results of rock mass quality based on RMR.

Depth/m	UCS	RQD	Spacing	Joint Condition	Ground Water	Revision	RMR	Rock	Rock Quality
−1465	5	20	10	21	4	−5	55	III	fair

The geological strength index (GSI) was first proposed by Hoek in 1995 and developed in engineering rock mechanics [29]. It can be used to directly estimate the strength and deformation modulus of a rock mass by using the mechanical properties of rock and some results of rock mass observation. Since Hoek proposed GSI, it has been continuously enriched and developed in practical engineering applications. Through the accumulation of a large amount of practical engineering experience, the RMR and Q can be directly transformed to the GSI [30], which can be calculated by the following expression:

$$GSI = RMR - 5 \quad RMR > 23 \quad (2)$$

$$GSI = 0.7RMR + 22.3 \quad (3)$$

$$GSI = 9\ln Q' + 44 \quad (4)$$

In Equation (4), $Q' = (RQD/J_n)\cdot(J_r/J_a)$, that is, Q when both J_w and SRF are 1. The results are listed in Table 4.

Table 4. Rock mass quality evaluation results based on GSI.

Calculation Method	GSI	Average
RMR	50	60
	61	
Q	70	

Rock mass properties, such as the Hoek–Brown constant, UCS (σ_{cmass}) and uniaxial tensile strength of the rock mass (σ_{tmass}), deformation modulus (E_m) and shear strength parameters, were calculated according to laboratory rock mechanics tests and field investigations, combined with the Hoek–Brown failure criterion [31]. Considering the influence of blasting and excavation disturbance on the mechanical properties of the rock mass, the excavation disturbance factor D was conservatively taken as 0.8, and the mechanical

parameters of the rock mass at −1465 m depth were estimated via RocLab software, as shown in Table 5.

Table 5. Mechanical parameters of the rock mass.

GSI		m	s	a	φ/°	c/MPa	σ_{cmass}/MPa	σ_{tmass}/MPa	E_m/GPa
Peak	60	7.669	0.0117	0.503	43.58	12.025	16.019	0.229	35.693
Residual	30	2.627	0.0004	0.522	64.02	7.876	2.575	0.024	5.586

3. Shaft Support Design

The selection of the shaft support system needs to specify the safe self-stabilization span and the maximum unsupported stand-up time. In rock masses with different excavation spans and different quality grades, the stand-up time of the shaft varies greatly. In a poor rock mass without support, the surrounding rock will instantaneously collapse. The maximum stand-up time and the safe self-stabilization span of the shaft can be estimated based on the RMR, as shown in Figure 5 [28]. It can be seen from the figure that the safe self-stabilizing span of the shaft is 2.8 m and the maximum stand-up time is 200 h, which obviously cannot meet the requirements of a metal mine for the stability of the shaft, so it is necessary to select appropriate support for it.

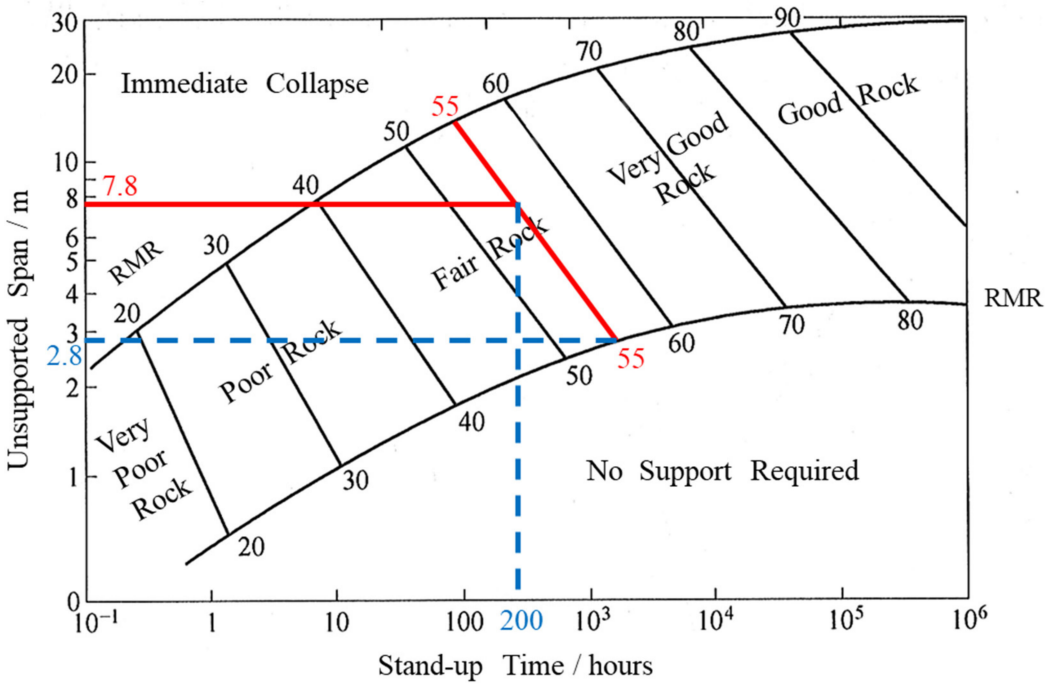


Figure 5. Maximum self-stabilization span and time of unsupported rock mass based on RMR.

The surrounding rock support pressure of the shaft mainly includes the surrounding rock deformation pressure and loose surrounding rock pressure. In the existing support schemes, the shaft is supported by a C50 concrete single lining with a lining thickness of 0.5 m. The lining support is rigid passive support. For deep surrounding rock, this support method cannot resist the damage caused by high stress by increasing the bearing strength of the surrounding rock itself, and it is difficult to achieve the coupling state between the lining and surrounding rock mass, which will lead to the formation of a high stress concentration area locally in the shaft, which is not conducive to the stability of the surrounding rock. In addition, considering the deformation pressure of the rock around the shaft, the support force of the support system should be increased accordingly. However, if the support system adopts rigid support, it will lead to the failure of the effective release of deformation energy in the rock around the shaft, which easily induces rock burst. Therefore,

it is necessary to release the deformation pressure of the surrounding rock in a stable and controllable way through initiative support. Bolts are a common initiative support method for surrounding rock. The engineering analogy method is usually adopted, which is the main surrounding rock support design method of underground engineering based on the geological and mechanical classification of rock masses via Q and the RMR [28]. To relate the Q system to the excavation form and support requirements, Barton defines an additional parameter [25]:

$$D_e = \frac{B}{ESR} \tag{5}$$

where D_e is a function of excavation size and excavation support ratio and B is the shaft span (m). ESR is the excavation support ratio. The ESR is related to the use of excavation and the safety level of the support system. The higher the safety level, the greater the ESR. The range of ESR values is generally 0.8~5.0 [25].

For the −1465 m shaft, the ESR is 1.6. The length of the rock bolt could be estimated according to the excavation support ratio ESR [25]:

$$L_b = 2 + 0.15B/ESR \tag{6}$$

where L_b is the bolt length (m).

Based on the above analysis, the shaft support scheme is shown in Table 6.

Table 6. Design of the bolting and shotcrete support bolt mesh and shotcrete layer thickness.

Basis	Q Recommended Support	RMR Recommended Support	Final Support
Parameter (ESR = 1.6; D_e = 7.8)	Bolt support $L_b \times S_b$ = 2.4 × 1.3 m	Bolt shotcrete support $L_b \times S_b$ = 4 × 1.5 m Concrete spray layer thickness 0.05 m	Bolt shotcrete support $L_b \times S_b$ = 4 m × 1.3 m, L_a = 2 m; Concrete spray layer thickness 0.05 m
Description	L_b is the length of the bolts; S_b is the distance between the rows of bolts; L_a is the anchoring length of the bolts		

Concrete lining is often used for permanent shaft support. The combination of lining and bolt shotcrete support can make the support system and shaft wall form an effective load-carrying structure to resist shaft crushing failure possibly caused by deep in situ stress. For shaft concrete linings, the lining pressure and lining thickness should be determined. In 1983, based on his coal mine research, Unal proposed Equation (7), which is used to calculate the support pressure of the surrounding rock lining through the RMR [32]. Barton plotted the relationship between the support pressure of 200 underground chambers and Q and proposed Equation (8), which can be used to calculate the support pressure of the surrounding rock lining [25]. The theoretical concrete lining thickness can be calculated according to Equation (9), which could be used to check the main shaft design lining thickness of the Shaling Gold Mine [33].

$$P = \left[\frac{100 - RMR}{100}\right] \cdot \gamma \cdot B \tag{7}$$

where P is the lining pressure (MPa) and γ is the unit bulk density of the rock mass (MN/m^3).

$$P = \frac{0.2}{J_r} \cdot Q^{-\frac{1}{3}} \tag{8}$$

$$t = R\left[\left(\frac{\frac{\sigma_{ch}}{SF}}{\frac{\sigma_{ch}}{SF} - 2P}\right)^{\frac{1}{2}} - 1\right] \tag{9}$$

where σ_{ch} is the uniaxial compressive strength of concrete (50 MPa for C50 concrete), R is the inner diameter of the main shaft (m), t is the thickness of the concrete lining (m) and SF is the safety factor of concrete lining failure. In this study, SF is 2.5.

According to the above, the calculation results are listed in Table 7. The results prove that the design support pressure of the original C50 concrete lining completely meets the safety requirements of the shaft lining.

Table 7. Calculated lining pressure and thickness.

Equation (7)	Equation (8)	Theoretical Pressure/MPa	Theoretical Thickness/m	Design Pressure/MPa	Design Thickness/m
0.093	0.055	0.074	0.015	1.36	0.5

4. Stability Analysis of Shaft Support via Numerical Simulation

4.1. Numerical Model Establishment

The finite element numerical simulation software Phase2 was used to test the plastic region range and displacement distribution of the surrounding rock with different support systems in the shaft with a depth of 1465 m to verify the application effect of the selected support system. At present, most numerical calculations are carried out under a series of simplified and assumed conditions. Before the finite element numerical simulation of the shaft, it was assumed that the rock mass was a continuous, homogeneous, isotropic medium and conforms to the Hoek–Brown failure criterion. The physical and mechanical parameters of the rock mass were determined according to Table 5. The solution accuracy of the numerical simulation was closely related to the selection of the boundary size. Due to the influence of the boundary effect, the selection of the model boundary was too small, which may have led to a large difference between the final simulation results and the real results. To improve the calculation accuracy, the boundary size was selected as 140 m × 140 m, a six-node triangular division unit was adopted, the grid type was a classified system, the classification factor was 0.05, and the surrounding rock of the shaft wall was densified. A total of 5556 nodes and 2684 triangular elements were divided. The maximum horizontal principal stress of the surrounding rock was 45.8 MPa, the direction was NW65°, the minimum horizontal principal stress was 37.6 MPa, and the vertical principal stress was 40.5. Zero displacement constraints were added in the horizontal and vertical directions to establish the numerical model of the shaft, as shown in Figure 6, and the shaft support model of the lining support, bolt shotcrete support, bolt shotcrete and lining combined support was established, as shown in Figure 7.

4.2. Analysis of the Plastic Region

Figure 8 shows the shape of the plastic region in the shaft without support and under different support conditions. Different colors indicate the damage degree of the surrounding rock after excavation. In the unsupported state, the initial plastic region radius of the shaft was 6.5 m, and the plastic region radii under the three supporting conditions were 6.1 m, 5.6 m and 5.1 m. The radius of the plastic region of the shaft was significantly reduced after the adoption of different support systems. Among them, the bolt shotcrete and lining combined support showed the best control effect on the plastic failure of the surrounding rock of the shaft. Compared with the unsupported condition, the plastic region scope was reduced by 22%. The number of yielded elements of the rock mass was reduced from 440 to 142. It can be seen from Figure 8b that the maximum axial force and minimum axial force of the concrete in the existing lining support of the shaft were 23.78 MPa and 1.06 MPa, respectively, meaning that C50 concrete could meet the stability requirements of the shaft.

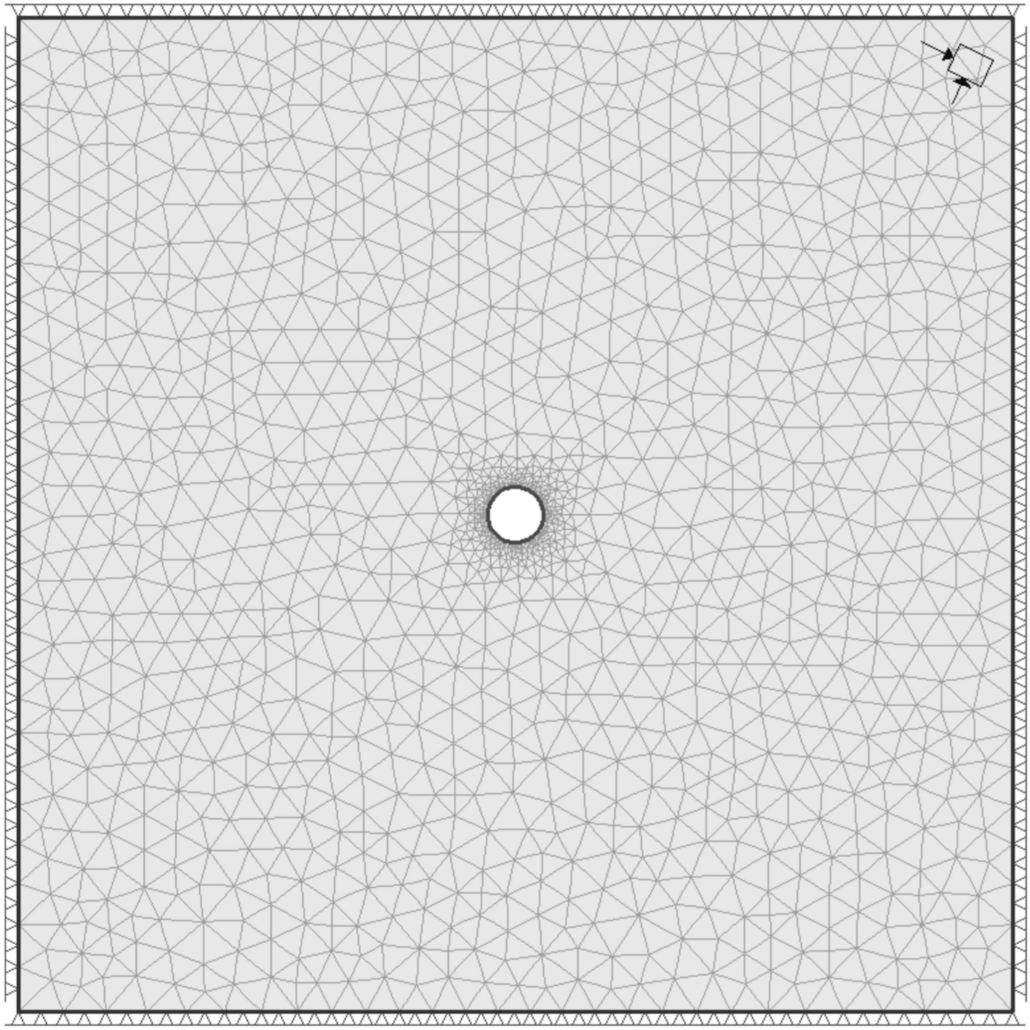
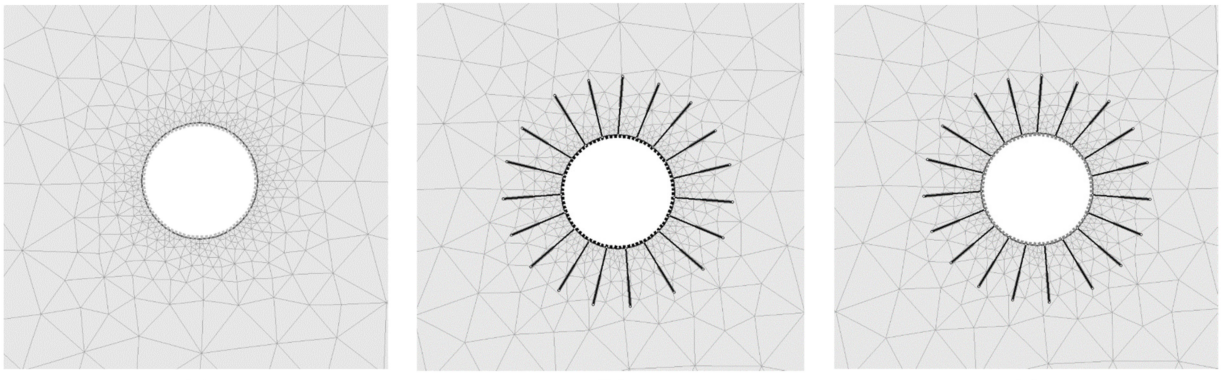


Figure 6. Shaft numerical calculation model.



(**a**) (**b**) (**c**)

Figure 7. (**a**) Lining support; (**b**) bolt shotcrete support; (**c**) bolt shotcrete and lining support.

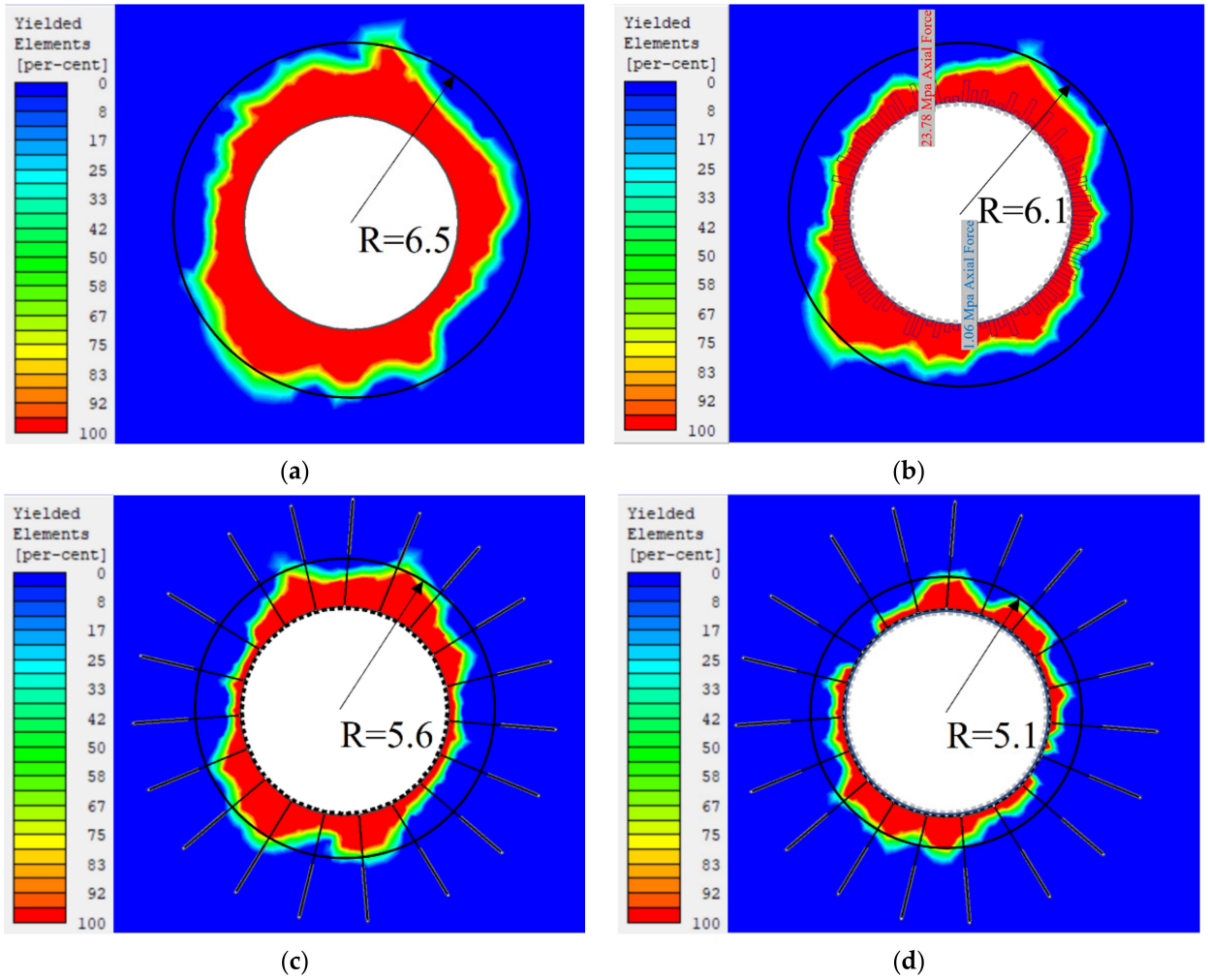


Figure 8. (**a**) Without support; (**b**) lining support; (**c**) bolt shotcrete support; (**d**) bolt shotcrete and lining support.

4.3. Analysis of the Displacement

Figure 9 shows the shaft wall displacement curves without support and with different support forms. The distance of the abscissa represents the length from the origin along the anticlockwise direction of the shaft wall with the top point on the left side of the shaft wall as the coordinate origin. Figure 9 shows that the shaft wall displacement was 0.656 m~1.013 m without support, and the maximum displacement was 4.9 m away from the origin. It can be seen from Figure 10 that the displacement of the shaft wall significantly decreased after the support, and the trend of displacement of the shaft wall with different support forms was roughly the same, with peaks appearing at 4~5 m and 16~18 m away from the origin, and the connecting line of the two peak points was basically perpendicular to the direction of the maximum horizontal principal stress. Lining support can only depend on the bearing strength of concrete itself to prevent the deformation and destruction of surrounding rocks. Rigid support easily accumulates deformation energy between the surrounding rocks and the concrete of the shaft and causes high levels of deformation and destruction. Bolt shotcrete support can make the support structure and surrounding rock form an integral part and form a compression arch structure inside the surrounding rock, thus increasing the mechanical properties of weak surrounding rock to resist the damage caused by high stress. Lining and bolt shotcrete support can give full play to the mechanical characteristics of concrete and enhance the bearing strength of the surrounding rock mass itself to achieve the best support effect. The higher the support level is, the smaller the

displacement of the shaft wall. After the combined support of bolt shotcrete and lining, the maximum displacement of the shaft wall was only 0.045 mm.

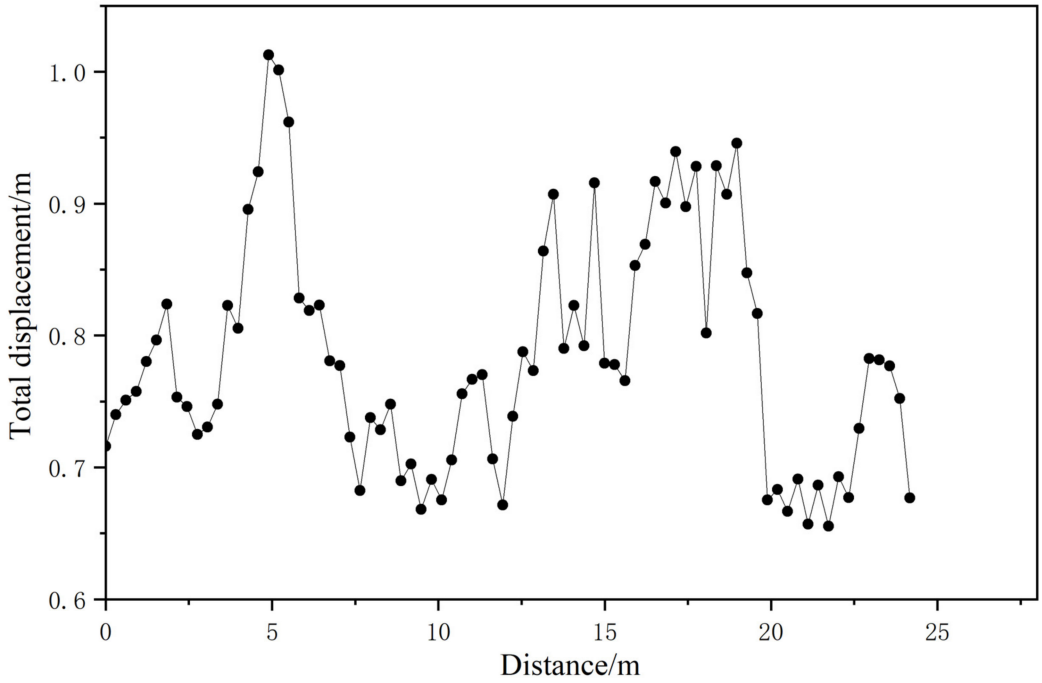


Figure 9. Displacement curve of the shaft without support.

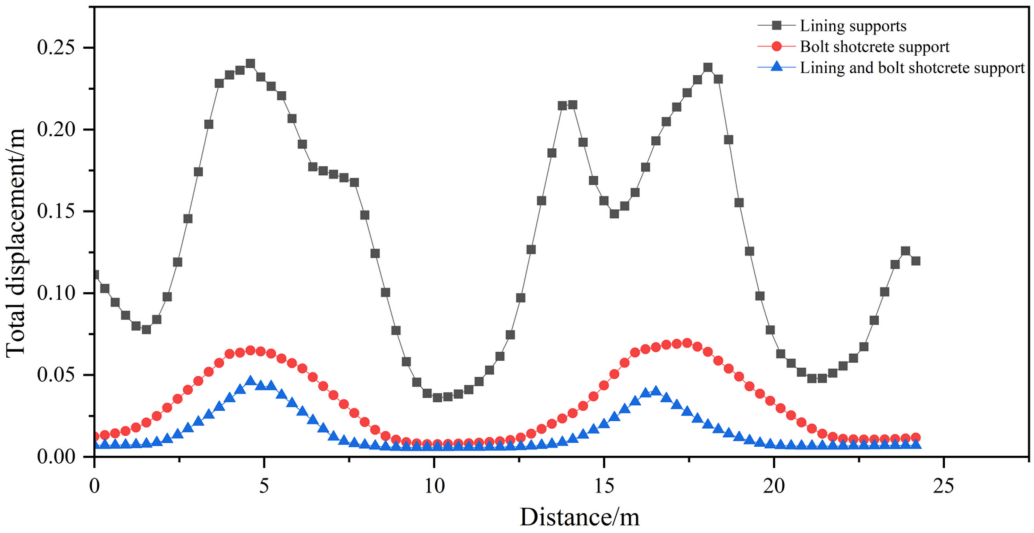


Figure 10. Displacement curves of the shaft with different supports.

5. Analytical Solutions of Shaft Surrounding Rock

5.1. Mechanical Model of Rock Mass

Figure 11 shows the circular opening with radius R_0 in the infinite rock mass, which is subject to the hydrostatic in situ stress σ_0 [34,35]. The surrounding rock is a homogeneous and isotropic elastic brittle plastic rock mass. The support system provides uniform radial support resistance p_0. After section excavation, the surrounding rock will produce a plastic region with a radius of R_p. The stress–strain and ε_r—ε_θ relationship of the rock mass can be described by the model in Figure 12 [36,37].

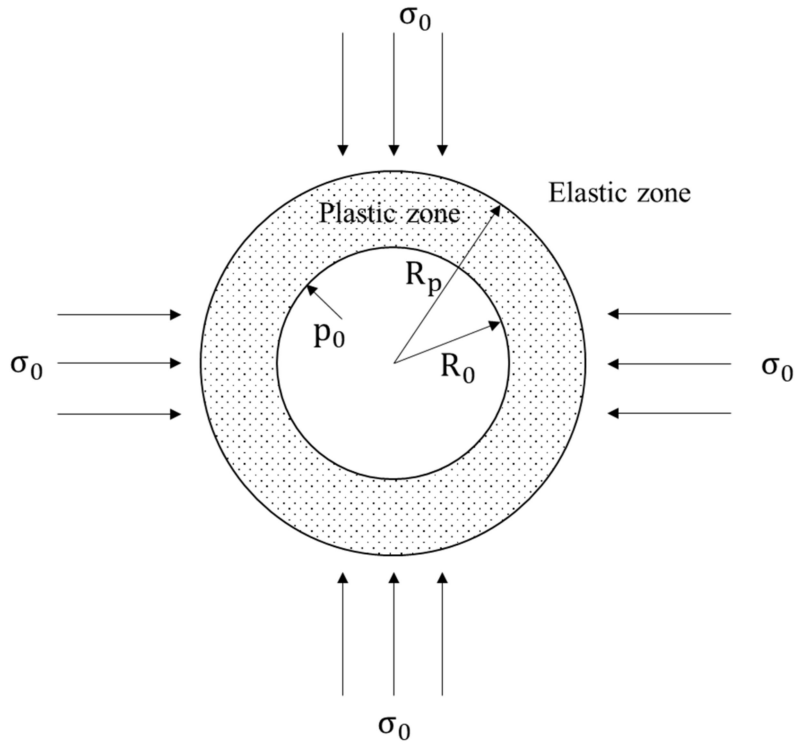
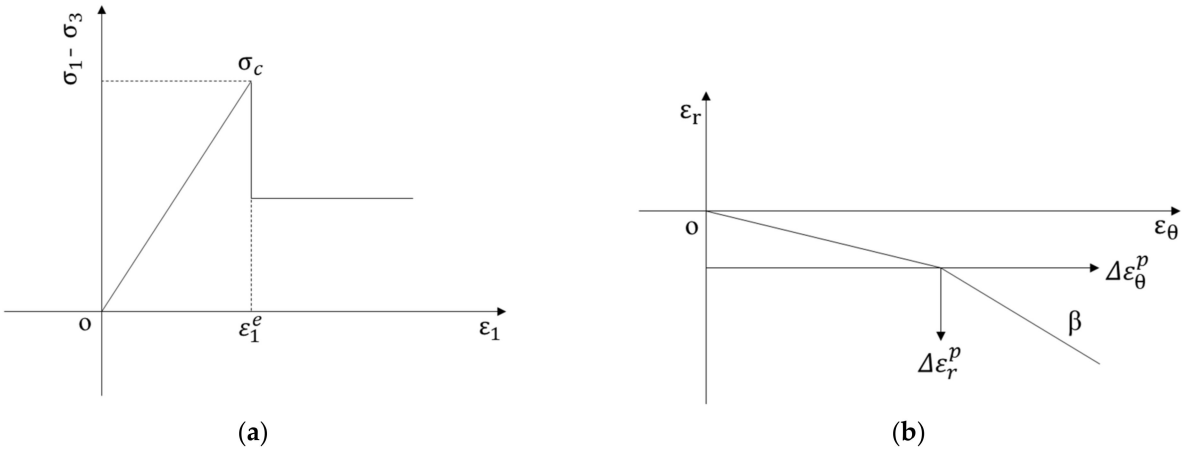


Figure 11. Mechanical model of hard rock shaft.



(**a**) (**b**)

Figure 12. (**a**) Elastic–brittle–plastic constitutive curve. (**b**) ε_r—ε_θ strain curve.

The rock mass is assumed to be governed by the Hoek–Brown failure criterion given by [31]:

$$\sigma_1 = \sigma_3 + \sqrt{m\sigma_c\sigma_3 + s\sigma_c^2} \quad (10)$$

where σ_1 and σ_3 are the maximum principal stress and the minimum principal stress, respectively, σ_c is the uniaxial compressive strength of intact rock, m is the Hoek–Brown constant, and s is the empirical parameter of the degree of rock fragmentation.

For the surrounding rock environment of shaft excavation, $\sigma_1 = \sigma_\theta$, $\sigma_3 = \sigma_r$; σ_θ and σ_r are the tangential stress and radial stress of the surrounding rock, respectively, so Equation (10) can be written as:

$$\sigma_\theta = \sigma_r + \sqrt{m\sigma_c\sigma_r + s\sigma_c^2} \quad (11)$$

The stress equilibrium equation of any element in the shaft surrounding rock under polar coordinates is:

$$\sigma_\theta = \sigma_r + r\frac{d\sigma_r}{dr} \tag{12}$$

The geometric equation is:

$$\varepsilon_r = \frac{du}{dr}, \varepsilon_\theta = \frac{u}{r} \tag{13}$$

where u is the radial displacement of the shaft surrounding rock and ε_r and ε_θ are the radial and tangential strains of the surrounding rock, respectively.

According to Figure 12, referring to the flow rule of rock mass dilatancy:

$$\Delta\varepsilon_r^p = -\beta\Delta\varepsilon_\theta^p \tag{14}$$

where $\Delta\varepsilon_r^p$ and $\Delta\varepsilon_\theta^p$ are the radial and tangential plastic strain increments in the plastic region of the surrounding rock, and β is the volumetric dilatancy parameter of the surrounding rock, $\beta = (1 + \sin\varphi)/(1 - \sin\varphi)$.

5.2. Strains and Displacement of the Elastic Region

According to the theory of elasticity [34,35]:

$$\sigma_r^e = \sigma_r^R\left(\frac{R_p}{r}\right)^2 + \sigma_0\left[1 - \left(\frac{R_p}{r}\right)^2\right] \tag{15}$$

$$\sigma_\theta^e = -\sigma_r^R\left(\frac{R_p}{r}\right)^2 + \sigma_0\left[1 + \left(\frac{R_p}{r}\right)^2\right] \tag{16}$$

$$u^e = (\sigma_0 - \sigma_r^R)\left(\frac{1+\nu}{E}\right)\left(\frac{R_p^2}{r}\right) \tag{17}$$

$$\sigma_r^R = \left|\frac{(2\sigma_0 - \sigma_c)}{1+\beta}\right| \tag{18}$$

where σ_r^e and σ_θ^e are the radial and tangential stresses in the elastic region, respectively, u^e is the radial displacement of the elastic region, σ_0 is the situ stress of the rock mass, R_p is the radius of the plastic region, and σ_r^R is the radial stress when $r = R_p$.

By substituting Equation (17) in Equation (13):

$$\varepsilon_\theta^e = -\varepsilon_r^e = \left(\sigma_0 - \sigma_r^R\right)\left(\frac{1+\nu}{E}\right)\left(\frac{R_p}{r}\right)^2 \tag{19}$$

where ε_θ^e and ε_r^e are the tangential and radial strains of the elastic region, respectively.

5.3. Stress Displacement and Radius of the Plastic Region

By substituting Equation (11) in Equation (12):

$$\frac{d\sigma_r}{dr} = \frac{\sqrt{m\sigma_c\sigma_r + s\sigma_c^2}}{r} \tag{20}$$

When $r = R_0$, $\sigma_r = p_0$. By substituting Equation (19), the radial stress of the surrounding rock in the plastic region can be obtained as:

$$\sigma_r^p = \frac{\left(\sqrt{m\sigma_c p_0 + s\sigma_c^2} - \frac{m\sigma_c \ln\frac{R_0}{r}}{2}\right)^2 - s\sigma_c^2}{m\sigma_c} \tag{21}$$

Equation (20) is substituted into Equation (11) to obtain σ_θ^p.

The total strain in the plastic region is:

$$\varepsilon_r^p = \varepsilon_r^{e'} + \Delta\varepsilon_r^p \tag{22}$$

$$\varepsilon_\theta^p = \varepsilon_\theta^{e'} + \Delta\varepsilon_\theta^p \tag{23}$$

where ε_r^p and ε_θ^p are the radial and tangential strains of the plastic region, respectively, and $\varepsilon_r^{e'}$ and $\varepsilon_\theta^{e'}$ are the radial and tangential elastic strains when $r = R_p$, respectively.

By combining Equations (13), (14), (19) and (20):

$$\frac{du}{dr} + \beta\frac{u}{r} = \left(\sigma_0 - \sigma_r^R\right)\left(\frac{1+\nu}{E}\right)(\beta - 1) \tag{24}$$

According to Equation (17), when $r = R_p$, $u = (\sigma_0 - \sigma_r^R)((1 + \nu)/E)\, R_p$, then:

$$u^p = \frac{2\alpha r}{1+\beta}\left[\frac{1+\beta}{2} + \left(\frac{R_p}{r}\right)^{1+\beta} - 1\right] \tag{25}$$

where $\alpha = (\sigma_0 - \sigma_r^R)((1 + \nu)/E)$.

When $r = R_p$, $\sigma_r = \sigma_r^R$. By substituting Equation (21), the radius of the plastic region can be obtained as:

$$R_p = \frac{R_0}{\exp\left[\frac{2\left(\sqrt{m\sigma_r^R\sigma_c + s\sigma_c^2} - \lambda\right)}{m\sigma_c}\right]} \tag{26}$$

where $\lambda = \sqrt{m\sigma_c p_0 + s\sigma_c^2}$.

The residual value of the rock mass mechanical parameters, net diameter of the shaft and C50 concrete support force are substituted into Equation (26). The parameters required in the calculation process are shown in Table 8. Under the condition of lining support, the radius of the plastic zone of the shaft surrounding rock was approximately 6.66 m.

Table 8. Calculation parameters of the plastic region radius of the lining support.

R_0/m	m	s	σ_0/MPa	φ/°	σ_c/MPa	p_0/MPa	σ_r^R/MPa
3.9	2.627	0.0004	45.8	64.02	149.7	50	3.09

6. Determination of Plastic Region Range by Acoustic

The propagation velocity of ultrasonic waves in geotechnical media is related to the physical and mechanical indexes of the structure. The greater the stress of the surrounding rock, the denser the rock mass and the fewer the cracks, the faster the ultrasonic wave will propagate in the rock mass [38–40]. Therefore, the range of the plastic region of the shaft could be determined by using the P-wave velocity test, and the test instrument was RSM-RCT(B). The acoustic emission hole and receiving hole were drilled on the shaft wall at a depth of −1465, and the angle of position was 90°, 135°, 225°, 270° and 340°, as shown in Figure 13. The aperture should have been 0.04 m, the spacing between the transmitter and the receiver should have been 0.3 m, and the drilling depth should have been 4 m. Clear water was required as the coupling medium to accurately measure the P-wave velocity of the surrounding rock mass and to continuously inject water into the hole to ensure that the whole hole could be filled with water, as shown in Figure 14.

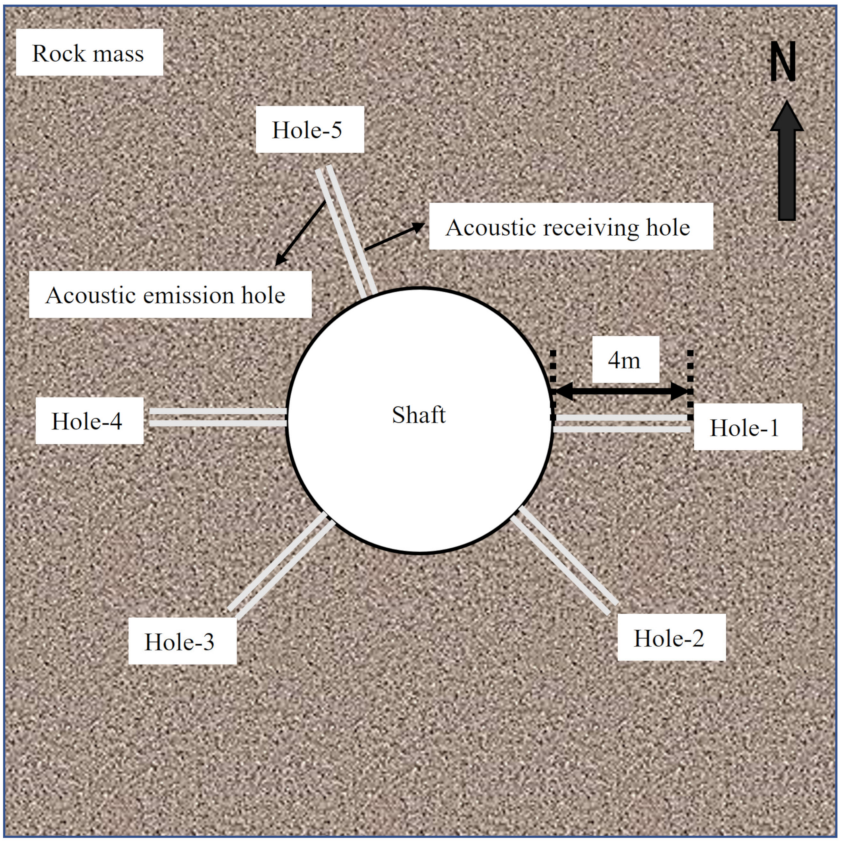


Figure 13. Arrangement of test holes in the plastic region of the shaft.

According to the principle of P-wave propagation in Figure 14, the wave velocity at different depths from the orifice was calculated by dividing the distance from the emission hole to the receiving hole by the propagation time of the sound wave from the transmitter to the receiver, and the relationship curve between the wave velocity and the depth of the measuring hole could be obtained. The thickness and range of the plastic region could be obtained in combination with the specific conditions of the surrounding rock, and the field test process is shown in Figure 15.

According to the principle of the acoustic velocity detection method, the inflection point of the wave velocity change could be used as the boundary between the elastic region and plastic region of the surrounding rock. According to Figure 16, the thicknesses of the plastic region corresponding to the surrounding rock with shaft azimuths of 90°, 135°, 225°, 270° and 340° were 0.8 m, 1.3 m, 2.2 m, 2.8 m and 0.7 m, respectively. Thus, the shape of the −1465 m plastic region of the main shaft in the Shaling Gold Mine could be obtained as shown in Figure 17. The maximum failure depth of the shaft's plastic region was 2.8 m, the angle was 225° and the radius of the plastic region was 6.7 m.

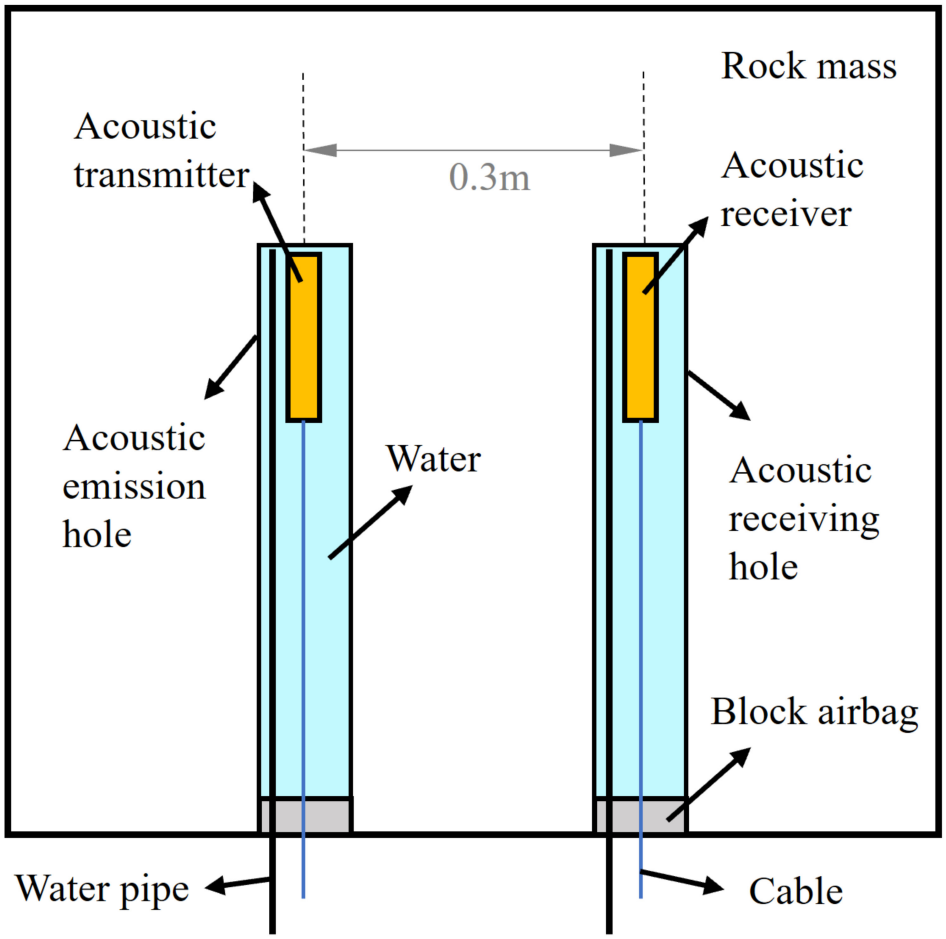


Figure 14. Principle of the P-wave velocity test.



Figure 15. Field test process.

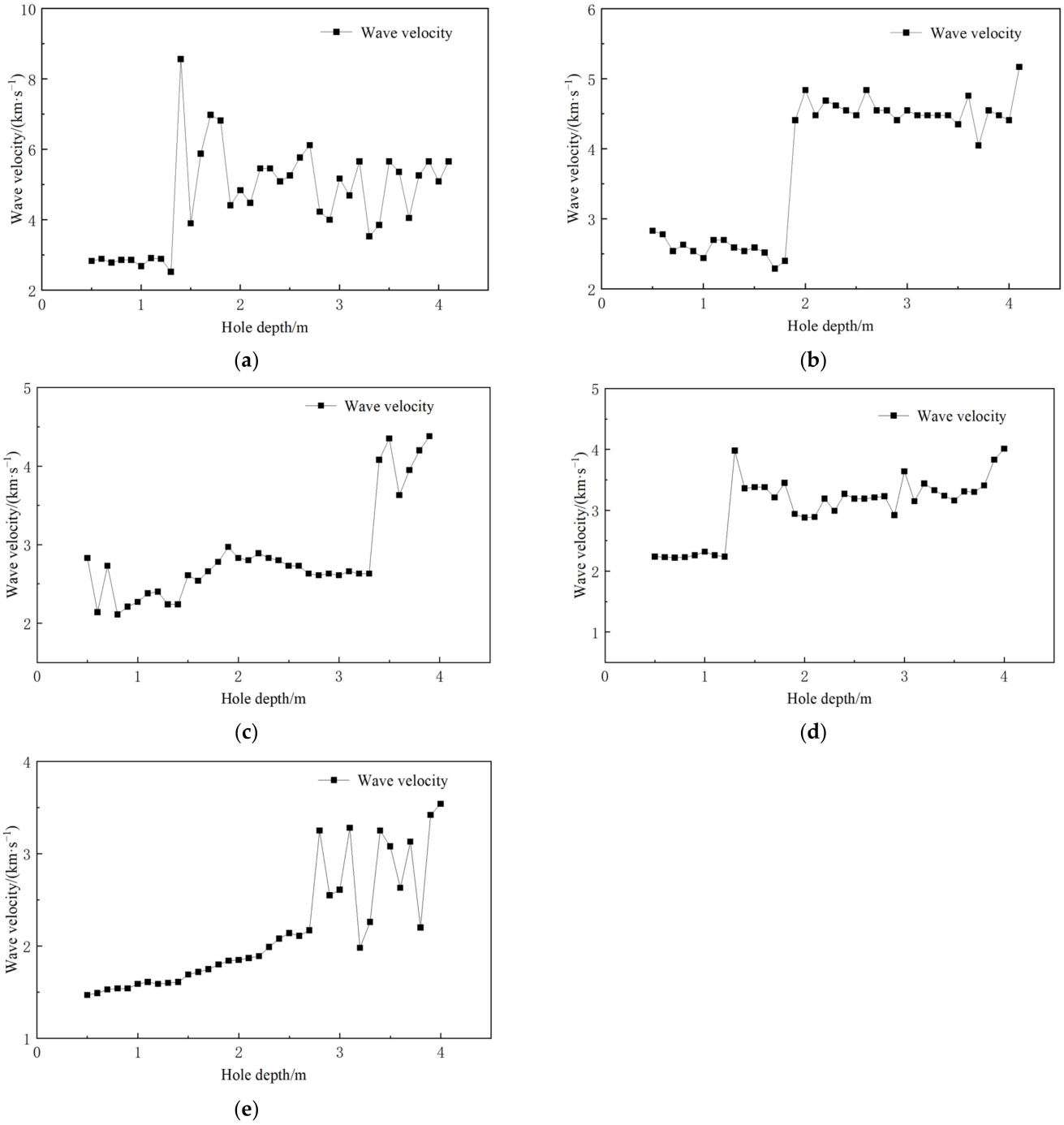


Figure 16. P-wave velocity test curve. (**a**) Hole 1; (**b**) Hole 2; (**c**) Hole 3; (**d**) Hole 4; (**e**) Hole 5.

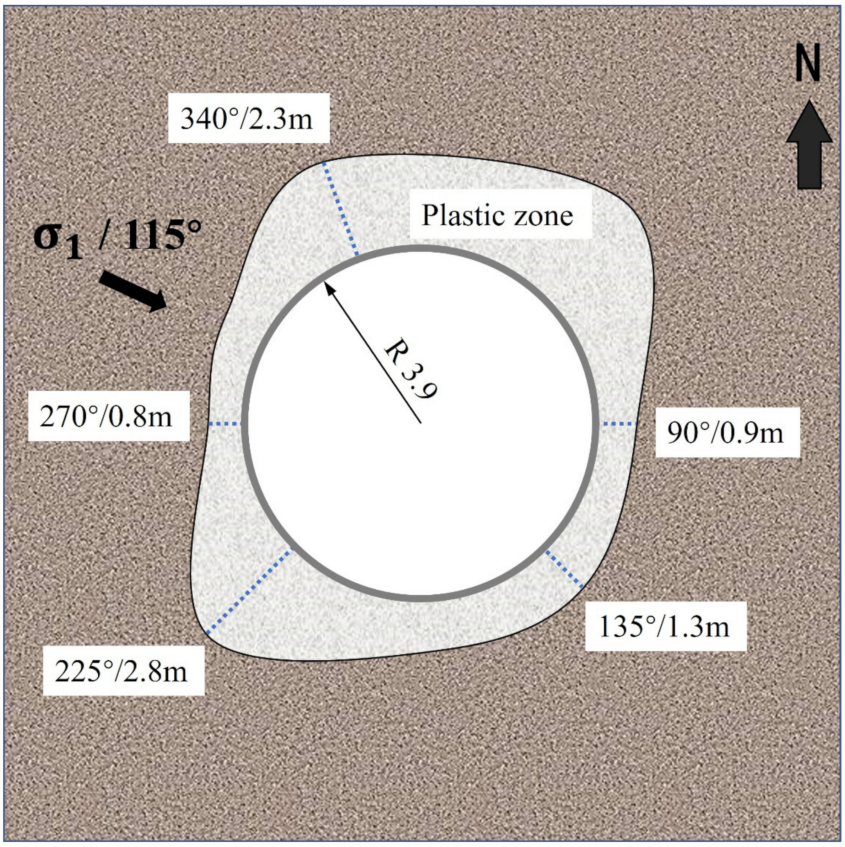


Figure 17. Delineation of the plastic region range.

7. Conclusions

Based on the finite element numerical simulation, theoretical analysis and field test, a comprehensive stability analysis of the surrounding rock in the deep section of the main shaft of Shaling was carried out. The main conclusions are as follows:

- For the deep section of the main shaft, the best supporting effect can be achieved by adopting the bolt shotcrete and lining combined support. According to the numerical simulation results, the maximum displacement of the surrounding rock of the shaft can be reduced to 0.045 m, and the radius of the plastic region can be reduced by 22% compared with the unsupported state.
- Under the condition of lining support, the numerical simulation, theoretical calculation and field measurement results of the radius of the shaft plastic region are 6.1 m, 6.66 m and 6.7 m, respectively. After comprehensively considering the dilatancy and plastic softening characteristics of the hard rock mass, the theoretical calculation value of the plastic region of the shaft is consistent with the measured result, which indicates that the mechanical characteristics of the rock mass should be fully considered in the stability analysis of the surrounding rock of underground engineering, and the combination of multiple analysis methods can better reveal the actual state of the surrounding rock.
- Numerical simulation and p-wave test results show that the direction of the maximum depth of the surrounding rock plastic region is basically perpendicular to the direction of the maximum principal stress, which verifies the accuracy of the main shaft situ stress measurement results.

Author Contributions: Funding acquisition, X.Z.; writing—review and editing, S.Q.; investigation, S.Q., Y.L., W.Y. and T.W. All authors have read and agreed to the published version of the manuscript.

Funding: This work was supported by a project of the NSFC Shandong United Fund (U1806208) and the Key projects of National Natural Science Foundation of China (52130403), the Fundamental Research Funds for the Central Universities (N2001033 and N2101022).

Institutional Review Board Statement: Not applicable.

Informed Consent Statement: Not applicable.

Data Availability Statement: Data sharing not applicable.

Conflicts of Interest: All the authors declare that they have no known conflicts of interest that could influence the work reported in this paper.

References

1. Xie, H.P.; Gao, F.; Ju, Y. Research and development of rock mechanics in deep ground engineering. *Chin. J. Rock Mech. Eng.* **2015**, *11*, 2161–2178. [CrossRef]
2. Liang, L.H. The Study on Wall Rock Stability and Supporting Structure of High-Buried Underground Cavern. Ph.D. Thesis, Tianjin University, Tianjin, China, 2007. [CrossRef]
3. Sun, B. Micromechanics Study on the Failure Mechanism and Stability of Deep Buried Surrounding Rock of Underground Cavern. Ph.D. Thesis, Tianjin University, Tianjin, China, 2012. [CrossRef]
4. Wang, Y.L.; Liang, L.H.; Ji, C.L. Stability analysis of surrounding rock of high buried underground caverns. *Hai. Water Res.* **2009**, *6*, 51–53+57. [CrossRef]
5. Wu, D. *Research on Stability of Surrounding Rock during Deep Shaft Excavating*; Northeastern University: Boston, MA, USA, 2011. [CrossRef]
6. Guo, S.W.; Zhao, Q.H.; Zhang, Q. Application of BP artificial neural network in rock mass quality classification. *Ye. Riv.* **2015**, *1*, 111–114+118. [CrossRef]
7. Wang, B.; Chen, J.P.; Li, Z.X.; Chao, J. Application of artificial neural network in rock mass quality classification. *Wor. Geo.* **2004**, *1*, 64–68. [CrossRef]
8. Zhang, J.Y.; Guo, L.W.; Qiu, L.; Wang, F.S. Application of fuzzy mathematics theory in stability evaluation of coal mine roadway. *Min. Saf. Env. Pro.* **2007**, *4*, 23–25. [CrossRef]
9. Zhang, Y.J. Research on Tunnel Surrounding Rock Mass Stability and Risk Analysis Based on Uncertainty Theory. Ph.D. Thesis, Hunan University, Changsha, China, 2010. [CrossRef]
10. Hu, X.S.; Zhao, F.S.; Peng, Y.W. *Proceedings of the 3rd China Geotechnical and Engineering Academic Conference*; Sichuan Science and Technology Press: Chengdu, China, 2009; pp. 533–536.
11. Pan, C.; Zou, Y.; Chen, X.S.; Li, Q.; Wan, J.B. *Application and Development of Hydraulic Tunnel Technology*; Chin. Water&Power Press: Beijing, China, 2008; pp. 129–136.
12. Yan, T.; Li, K.J.; Mou, Z.H.; Zhang, J.X.; Yu, L.; Li, Q.; Peng, T. Analytical method for calculation of surrounding rock pressure of shallow-buried and unsymmetrically loaded tunnel adjacent to variable slope. *J. South. Jiao. Uni.* **2020**, *3*, 531–536. [CrossRef]
13. Zhun, J.F. Study on the Formation Mechanism and Its Engineering Application of Broken Rock Zone in Deep Bedded Rock Mass. Ph.D. Thesis, China University of Mining and Technology, Beijing, China, 2021.
14. Zhai, M.Y.; Sheng, J.L.; Ma, L.J. Numerical simulation analysis of stability of surrounding rock in tunnel based on Phase2. *Ind. Miner. Process.* **2017**, *3*, 46–48+71. [CrossRef]
15. Duan, Y.M.; Tao, Z.H.; Zhang, X.; Zhang, Y.Q. The numerical modeling study on the stability of underground backfill body and surrounding rock of Dahongshan copper mine. *Yun. Meta.* **2019**, *3*, 7–13. [CrossRef]
16. Jia, X.L. Study on numerical simulation of surrounding rock stability of deep roadway based on FLAC3D. *Chin. Ene. Env. Pro.* **2017**, *6*, 18–22. [CrossRef]
17. Wang, J.G. Study on numerical simulation of surrounding rock stability of roadway with dynamic pressure along gob. *Chin. Ene. Env. Pro.* **2019**, *1*, 130–134. [CrossRef]
18. Zhao, Y.M. Numerical simulation study on the influence of roadway section size on the stability of roadway surrounding rock. *Hyd. Coal Min. Pip. Tran.* **2018**, *3*, 24–26+29. [CrossRef]
19. Liang, H.B.; Li, Z.K.; Gu, Z.Q. FLAC and its application for hydropower projects in china. *Chin. J. Rock Mech. Eng.* **1996**, *3*, 6.
20. Ren, Q.W. Block element method and its application in rock mass stability analysis. *J. Hohai Uni. Nat. Sci.* **1995**, *1*, 1–7.
21. Chen, W.Z.; Zhu, W.S.; Wang, B.L.; Ren, W.Z. Numerical simulation and testing study of large deformation for cavern surrounding jointed rock mass. *Chin. J. Rock Mech. Eng.* **1998**, *3*, 223–229. [CrossRef]
22. Wu, A.Q.; Ren, F.; Dong, X.S. A study on the numerical model of dda and its preliminary application to rock engineering. *Chin. J. Rock Mech. Eng.* **1997**, *5*, 411–411. [CrossRef]
23. Tan, Y.L.; Jiang, F.X.; Fan, W.L.; Xu, E.H.; Liu, C.X. Simulation of bolting effect on the stability of jointed rockmass by dispersive elemet method. *J. Eng. Geo.* **1999**, *4*, 361–365. [CrossRef]
24. Pei, F. Mechanical Properties of Rock in Deep Stratum and Analysis and Control of Shaft Surrounding Rock Stability in Shaling Gold Mine. Ph.D. Thesis, University of Science and Technology Beijing, Beijing, China, 2020. [CrossRef]

25. Barton, N.; Lien, R.; Lunde, J. Engineering classification of rock masses for the design of tunnel support. *Rock Mech.* **1974**, *4*, 189–236. [CrossRef]
26. Grimstad, E.; Barton, N. Updating the Q-system for NMT. In Proceedings of the International Symposium on Sprayed Concrete-Modern Use of Wet Mix Sprayed Concrete for Underground Support, Fagerness, Norway, 22–26 October 1993; pp. 46–66.
27. Barton, N. Some new Q-value correlations to assist in site characterization and tunnel design. *Int. J. Rock Mech. Min. Sci* **2002**, *39*, 185–216. [CrossRef]
28. Bieniawski, Z. Engineering classification of jointed rock masses. *Civ. Eng. S. Afr.* **1973**, *15*, 333–343.
29. Hoek, E.; Brown, E.T. Practical estimates of rock mass strength. *Int. J. Rock. Mech. Min. Sci.* **1997**, *8*, 1165–1186. [CrossRef]
30. Yu, S.B.; Wang, H.; Cao, H. Discussion on correlation and application of various engineering rock mass quality evaluation methods. *Non. Meta. Min.* **2015**, *1*, 83–86. [CrossRef]
31. Eberhardt, E. The hoek–brown failure criterion. *Rock Mech. Rock Eng.* **2012**, *6*, 133–240. [CrossRef]
32. Unal, E. Modifed rock mass classifcation: M-RMR system. In *Milestones in Rock Engineering, the Bieniawski Jubilee Collection*; Bieniawski, Z.T., Ed.; Balkema: Rotterdam/Brookfeld, IL, USA, 1996; pp. 203–223.
33. Ozturk, H.; Unal, E. Estimation of lining thickness around circular shafts. In Proceedings of the 17th International Mining Congress and Exhibition of Turkey-IMCET2001, Ankara, Turkey, 19–22 June 2001; pp. 437–444.
34. Fu, G.B. A new study on the fracture range and displacement of roadway surrounding rock. *J. Chin. Coal Soc.* **1995**, *3*, 304–310.
35. Yuan, W.B.; Chen, J. Analysis of plastic zone and fracture zone of roadway in softened rock stratum. *J. Chin. Coal Soc.* **1986**, *3*, 77–86.
36. Wang, J.L.; Xiong, J.H. An analytical solution to cylindrical cavity expansion in softening soil mass. *Chin. J. Appl. Mech.* **1999**, *4*, 58–62+167.
37. Wang, X.H.; Wang, J.L.; Liang, F.Y. Analytical solution to the problem of hole enlarging in strain softening geotechnical materials. *Eng. Mech.* **1999**, *5*, 71–76.
38. Wang, J.Y. Test research on surrounding rock loose ring based on acoustic wave method. *Chin. Ene. Env. Pro.* **2017**, *12*, 272–274+278. [CrossRef]
39. Wu, T.; Dai, J.; Du, M.L.; Wu, Y.; Gao, Y.Z.; Yang, F. Surrounding rock loosing circle test based on acoustic test technology. *Safe. Coal Min.* **2015**, *1*, 4. [CrossRef]
40. Yang, X.X.; Wang, W.Q.; Jing, H.W. Analysis and coMParison on conventional loose zone measuring and test methods. *Coal Sci. Tech.* **2012**, *8*, 1–5+54. [CrossRef]

Disclaimer/Publisher's Note: The statements, opinions and data contained in all publications are solely those of the individual author(s) and contributor(s) and not of MDPI and/or the editor(s). MDPI and/or the editor(s) disclaim responsibility for any injury to people or property resulting from any ideas, methods, instructions or products referred to in the content.